N-terminal methionine excision of proteins creates tertiary destabilizing N-degrons of the Arg/N-end rule pathway

Received for publication, November 29, 2018, and in revised form, January 18, 2019 Published, Papers in Press, January 23, 2019, DOI 10.1074/jbc.RA118.006913

Kha The Nguyen, Jeong-Mok Kim, Sang-Eun Park, and Cheol-Sang Hwang[1]

From the Department of Life Sciences, Pohang University of Science and Technology, Pohang, Gyeongbuk 37673, Republic of Korea

Edited by Ursula Jakob

All organisms begin protein synthesis with methionine (Met). The resulting initiator Met of nascent proteins is irreversibly processed by Met aminopeptidases (MetAPs). N-terminal (Nt) Met excision (NME) is an evolutionarily conserved and essential process operating on up to two-thirds of proteins. However, the universal function of NME remains largely unknown. MetAPs have a well-known processing preference for Nt-Met with Ala, Ser, Gly, Thr, Cys, Pro, or Val at position 2, but using CHX-chase assays to assess protein degradation in yeast cells, as well as protein-binding and RT-qPCR assays, we demonstrate here that NME also occurs on nascent proteins bearing Met–Asn or Met–Gln at their N termini. We found that the NME at these termini exposes the tertiary destabilizing Nt residues (Asn or Gln) of the Arg/N-end rule pathway, which degrades proteins according to the composition of their Nt residues. We also identified a yeast DNA repair protein, MQ-Rad16, bearing a Met–Gln N terminus, as well as a human tropomyosin–receptor kinase–fused gene (TFG) protein, MN-TFG, bearing a Met–Asn N terminus as physiological, MetAP-processed Arg/N-end rule substrates. Furthermore, we show that the loss of the components of the Arg/N-end rule pathway substantially suppresses the growth defects of *naa20*Δ yeast cells lacking the catalytic subunit of NatB Nt acetylase at 37 °C. Collectively, the results of our study reveal that NME is a key upstream step for the creation of the Arg/N-end rule substrates bearing tertiary destabilizing residues *in vivo*.

Virtually all polypeptides emerging from ribosomes begin with methionine (Met), as this is the residue dictated by the translation initiation codons. The initiator N-terminal (Nt-)[2] Met of nascent polypeptides is co-translationally and irreversibly excised by ribosome-bound Met-aminopeptidases (MetAPs) if it includes a penultimate residue with a small and uncharged side chain (Ala, Gly, Ser, Cys, Thr, Pro, or Val) (1). Evolutionarily conserved Nt-Met (Nt-M) excision (NME) is applied to more than 50% of all nascent proteins, thus profoundly contributing to Nt-proteome diversity, enzyme activity, cell growth and viability, free Met or GSH homeostasis, etc. Nonetheless, the universal role of this massive NME process remains largely elusive (1–3).

In ~60% of nascent yeast proteins and 80% of nascent human proteins, the retained Nt-Met (Nt-M) and neo-Nt residues after NME very frequently undergo Nα-terminal acetylation (Nt-acetylation) (4). The Nt-M acetylation state of nascent proteins can be a primary decision-making step for the retention or removal of Nt-M, as it dynamically competes with NME on ribosomes by blocking MetAPs via steric hindrance (1, 4, 5). Moreover, numerous lines of evidence have uncovered that Nt-acetylation substantially contributes to protein stability, activity, folding, localization, and interaction, thus affecting cell proliferation, apoptosis, development, etc. (4, 6). Furthermore, Nt-acetylation elicits specific protein degradation signals (degrons), which are recognized directly by an Nt-acetylation–targeting proteolytic system, termed the Ac/N-end rule pathway (Fig. S1*B*) (6–8).

The common characteristic of the N-end rule pathways relies on the direct detection of protein Nt-degrons (N-degrons) by specific recognition components (N-recognins) for proteolysis (9). A critical and indispensable determinant of N-degrons is destabilizing residues, which are yielded either through their steric unmasking (via defects in the protein's folding, interaction, or localization, etc.) or subsequent Nt modifications (via acetylation, formylation, deamidation, oxidation, arginylation, endoproteolytic cleavage, etc.) (6, 9). In eukaryotes, specific ubiquitin (Ub) ligases or the autophagy adaptor SQSTM1 (p62) is a dedicated N-recognin of the N-end rule pathways and directly recognizes protein N-degrons, thereby mediating their degradation by 26S proteasomes or lysosomes (9, 10). The previously established N-end rule pathways in *Saccharomyces cerevisiae* are the Arg/N-end rule, Ac/N-end rule, Pro/N-end rule, and fMet/N-end rule pathways (see below) (Fig. S1, *A–D*) (6, 9, 11, 12).

The canonical N-end rule pathway is the Arg/N-end rule pathway, in which Nt-unacetylated destabilizing residues are

This work was supported by the Samsung Science and Technology Foundation Grant SSTF-BA1401-17, National Research Foundation of Korea (NRF) Grant NRF-2017R1A5A1015366 funded by the Korean Government (MSIP), the BK21 Plus Program, and the POSCO Green Science and Innovation Grant. The authors declare that they have no conflicts of interest with the contents of this article.

This article contains Fig. S1.

[1] To whom correspondence should be addressed. Tel.: 82-54-297-2352; Fax: 82-54-279-2291; E-mail: cshwang@postech.ac.kr.

[2] The abbreviations used are: Nt, N-terminal; NME, N-terminal methionine excision; MetAP, methionine aminopeptidase; Ub, ubiquitin; degron, degradation signal; CHX, cycloheximide; Nt-acetylation, N-terminal acetylation, qPCR, quantitative PCR; MEF, mouse embryonic fibroblast; PEI, polyethyleneimine; CAPS, 3-(cyclohexylamino)propanesulfonic acid; DMEM, Dulbecco's modified Eagle's medium; FBS, fetal bovine serum; PVDF, polyvinylidene difluoride; TFG, tropomyosin–receptor kinase–fused gene; ER, endoplasmic reticulum; ERAD, ER-associated protein degradation; Y2H, yeast two-hybrid.

targeted through a highly organized hierarchy (9). In *S. cerevisiae*, the primary destabilizing residues of the Arg/N-end rule pathway are type-1 basic (Arg, Lys, and His), type-2 bulky hydrophobic (Leu, Trp, Phe, Ile, and Tyr), or Met-Φ (a hydrophobic amino acid) Nt-residues (Fig. S1, *A* and *C*) (9, 13). The tertiary destabilizing residues Nt-Asn (Nt-N) and Nt-Gln (Nt-Q) are converted to the secondary destabilizing residues Asp and Glu, respectively, by Nta1 amidase (Fig. S1*A*). The resulting Nt-Asp (Nt-D) and Nt-Glu (Nt-E) are arginylated by Ate1 arginyltransferase. The sole N-recognin Ubr1 E3 Ub ligase (in concert with Ufd4 E3 Ub ligase) directly detects Nt-unacetylated type-1 basic and type-2 bulky hydrophobic residues for Ub-dependent and proteasome-mediated destruction in *S. cerevisiae* (9, 14). The Arg/N-end rule pathway performs a broad range of functions in protein quality control, small peptide sensing, chromosome segregation, DNA repair, stress responses, etc. (9, 15–21).

The Ac/N-end rule pathway destroys Nt-acetylated proteins via direct contact of their Nt-acetyl tag with the endoplasmic reticulum (ER)/nuclear transmembrane Doa10 (TEB4, also known as MARCH6, in mammals) or the cytosolic and nuclear Not4 E3 Ub ligases (Fig. S1*B*) (8, 22, 23). The Ac/N-end rule pathway has been implicated in the regulation of protein subunit stoichiometry, G-protein signaling–mediated blood pressure, circadian rhythms, plant stress responses, lipid droplet maintenance, etc. (13, 22–26).

Another branch of the N-end rule pathways is the Pro/N-end rule pathway, which directly targets Nt-Pro (Nt-P) or Pro at position 2 of a given protein, along with the adjacent sequences. The Pro/N-end rule pathway exploits Gid4 as a Pro/N-recognin, thereby degrading several gluconeogenic enzymes in *S. cerevisiae* (Fig. S1*D*) (11). The molecular structure and substrate specificity of human GID4 as the Pro/N-recognin have been recently determined (27).

The fMet/N-end rule pathway targets proteins carrying Nt-formyl-methionine (fMet) for degradation. We have recently found that fMet can be used to initiate protein synthesis in the cytosol of *S. cerevisiae* (12). The resulting fMet can also act as fMet/N-degron, in agreement with our previous prediction (8) and actual demonstration of its existence in bacteria (28). Of note, the eukaryotic fMet/N-end rule pathway recruits the Psh1 E3 Ub ligase as an fMet/N-recognin, thereby degrading cytosolic fMet-containing proteins via the Ub/proteasome system (Fig. S1*E*) (12).

Given their strong hydrolytic preference for Nt-Met-Gly (MG), Met-Ala (MA), Met-Ser (MS), Met-Cys (MC), Met-Thr (MT), Met-Val (MV), and Met-Pro (MP), MetAPs are generally postulated not to excise unmodified Nt-M bearing the tertiary-destabilizing residue Asn or Gln at position 2 (1). MetAP-generated neo-Nt residues are therefore widely assumed to be stabilizing in the context of the Arg/N-end rule pathway, with the exception of the Nt-C residue that becomes destabilizing through oxidation under certain circumstances (29–32). Interestingly, it has also been suggested that the prevention of NME may increase the protein life span because some plastid-encoded proteins become shorter-lived under conditions of reduced deformylation (33). On the contrary, this study reveals that NME substantially and discernibly occurs on proteins with tertiary-destabilizing residues, thus causing their degradation via the Arg/N-end rule pathway *in vivo*.

Results

Ubr1 mediates degradation of Nt-unacetylated MN-α2 fusions

The previously dissected reporter MN-$\alpha2^{3-67}$-e^K-ha-Ura3 (denoted as MN-α2-e^K-ha-Ura3) (8), generated by co-translational deubiquitylation of Ub^{R48}-MN-α2-e^K-ha-Ura3, contained Ub with a Lys-48 to Arg mutation (Ub^{R48}), Nt-MN, α2 (Nt-terminal 3–67 residues of a transcription repressor Matα2), a 44-residue e^K fragment (stemming from *Escherichia coli* LacI protein), the ha (YPYDVPDYA) tag, and the Ura3 (orotidine 5′-phosphate decarboxylase) reporter (Fig. 1*A*). The MN-α2-e^K-ha-Ura3 is Nt-acetylated *in vivo* by the NatB Nt-acetylase complex, which consists of a catalytic subunit Naa20 as well as an ancillary subunit Naa25, and is subsequently targeted for degradation by Doa10, an Ac/N-recognin of the Ac/N-end rule pathway (Fig. 1*A*) (8). Thus, *ura3*Δ (uracil auxotrophic) *S. cerevisiae* cells that expressed MN-α2-e^K-ha-Ura3 from the P_{CUP1} promoter on a low-copy-number plasmid with a *TRP1* auxotrophic marker grew very poorly on the synthetic complete SC-Trp-Ura (both tryptophan and uracil-lacking) medium because of the rapid degradation of the MN-α2-e^K-ha-Ura3 reporter (Fig. 1*B*). In agreement with our previous finding that Doa10 mediates degradation of MN-α2-e^K-ha-Ura3 by targeting its Nt-acetyl group (8), the loss of Doa10 notably rescued the growth of *ura3*Δ *S. cerevisiae* cells with MN-α2-e^K-ha-Ura3 on the same selective medium (Fig. 1*B*). Unexpectedly, the growth defect of the *ura3* yeast cells expressing MN-α2-e^K-ha-Ura3 was also markedly abolished by the absence of Ubr1, an N-recognin of the *S. cerevisiae* Arg/N-end rule pathway (Fig. 1*B*). Moreover, CHX-chase assays of protein degradation showed that MN-α2-e^K-ha-Ura3 was greatly stabilized in both *doa10*Δ cells (half-life ($t_{½}$) ≈74 min) and *ubr1*Δ cells ($t_{½}$ ≈81 min) compared with WT cells ($t_{½}$ ≈28 min) (Fig. 1, *C* and *D*).

The observed Ubr1- or Doa10 (via Nt-acetylation)-mediated degradation of MN-α2-e^K-ha-Ura3 was also retained in the otherwise identical reporter MN-$\alpha2^{3-67}$-GST (denoted as MN-α2-GST), containing GSH-*S*-transferase (GST) instead of the e^K-ha-Ura3 C-terminal moiety (Fig. 2*A*).

To elucidate the involvement of Ubr1 in the degradation of the reporter protein in more detail, we performed CHX-chase assays of MN-α2-GST in WT, *ubr1*Δ, *doa10*Δ, *ubr1*Δ *doa10*Δ, *naa20*Δ, and *naa20*Δ *ubr1*Δ cells via immunoblotting using anti-GST antibodies (which detect all species of MN-α2-GST variants). Indeed, analogous to our previous findings (8) and the above results with MN-α2-e^K-ha-Ura3 (Fig. 1), the MN-α2-GST was rapidly degraded in WT cells ($t_{½}$ ≈10 min), but partially stabilized in *ubr1*Δ ($t_{½}$ ≈30 min), *doa10*Δ ($t_{½}$ ≈21 min), or *naa20*Δ cells ($t_{½}$ ≈22 min) (Fig. 2, *B–E*). Strikingly, the short-lived MN-α2-GST was almost completely stabilized in either double-mutant *ubr1*Δ *doa10*Δ cells or *naa20*Δ *ubr1*Δ cells, demonstrating that the Arg/N-end rule and Ac/N-end rule pathways co-mediated the degradation of MN-α2-GST redundantly (Fig. 2, *B–E*).

To understand the impact of Nt-acetylation on the Ubr1-mediated degradation of MN-α2-GST more clearly, N-termi-

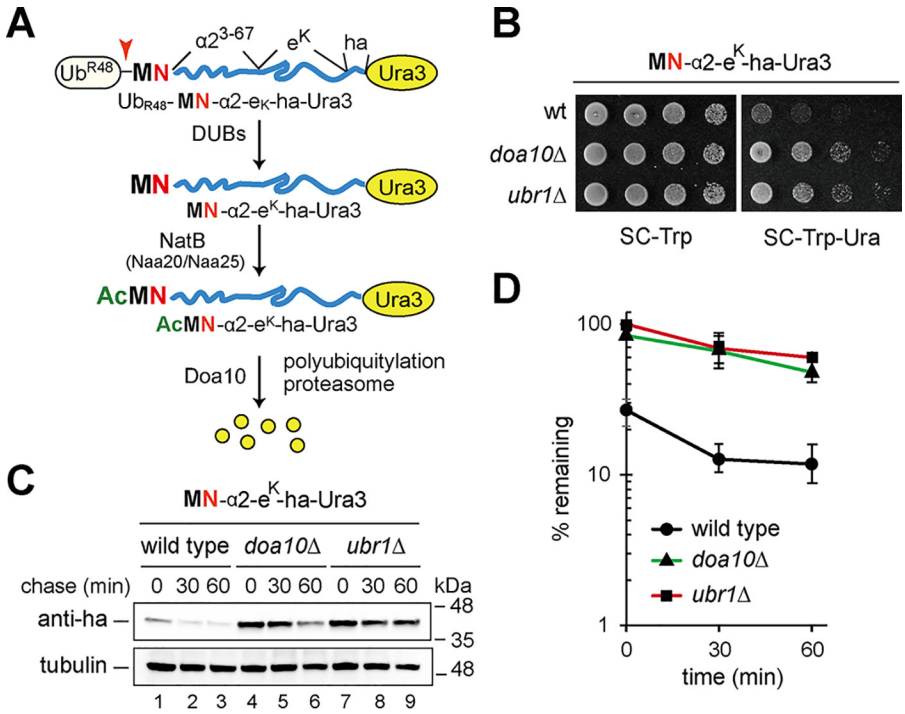

Figure 1. Ubr1 mediates degradation of MN-α2-e^K-ha-Ura3. *A*, scheme of the degradation of MN-α2-e^K-ha-Ura3 by the Ac/N-end rule pathway. Co-translational deubiquitylation of Ub^{R48}-MN-α2-e^K-ha-Ura3 yields MN-α2-e^K-ha-Ura3 *in vivo*. Degradation of the resulting MN-α2-e^K-ha-Ura3 involves NatB Nt-acetylase and Doa10 E3 Ub ligase. *B*, growth assays of WT, *doa10*Δ, or *ubr1*Δ cells expressing MN-α2-e^K-ha-Ura3. The indicated cells were cultured to A_{600} ≈1, serially diluted 5-fold, and then spotted on uracil-containing (SC−Trp) or uracil-lacking (SC−Trp−Ura) plates. The plates were incubated at 30 °C for 3 days. *C*, CHX chases of MN-α2-e^K-ha-Ura3 in WT, *doa10*Δ, or *ubr1*Δ *S. cerevisiae* for 0, 30, and 60 min. Cell extracts were separated by SDS/10% Tris-glycine PAGE, followed by immunoblotting with anti-ha and anti-tubulin antibodies. *D*, quantitation of data in *C*. Data show mean ± S.D. of three independent experiments.

nally FLAG-tagged Ubr1 (^{f}Ubr1) was transiently overexpressed from a P_{GAL1} promoter on a high-copy-number plasmid in *ubr1*Δ *doa10*Δ cells expressing MN-α2-GST from a P_{CUP1} promoter on a low-copy-number CEN plasmid (Fig. 2*F*). In particular, exponential cultures of the *ubr1*Δ *doa10*Δ cells in 2% raffinose-containing SRaf medium were allowed to grow for an additional 2.5 h after the addition of glucose (for *UBR1* repression) or galactose (for *UBR1* induction) to 2%. CHX-chase assays showed that the induction of ^{f}Ubr1 in the galactose-containing culture led to a significant decrease in the levels of total MN-α2-GST derivatives (Nt-acetylated, Nt-unacetylated, and other modified variants), but not in those of Nt-acetylated AcMN-α2-GST that was detected via immunoblotting with anti-α2^{AcM} antibodies (Fig. 2*F*) (8). Additionally, Nt-unacetylated MN-α2-GST (which, in fact, bore Nt-unacetylated or potentially processed MN-α2-GST derivatives. See below for details.) in *naa20*Δ *ubr1*Δ *doa10*Δ cells (lacking NatB Nt-acetylase) became markedly destabilized by the expression of ^{f}Ubr1, but not by that of the catalytically inactive mutant ^{f}Ubr1^{C1220S} (Fig. 2*G*). Furthermore, co-immunoprecipitation assays demonstrated that MN-α2-GST marginally, but detectably, interacted with ^{f}Ubr1 and more strongly interacted with catalytically inactive ^{f}Ubr1^{C1220S} (Fig. 2*H*). In actuality, the physical binding of ^{f}Ubr1^{C1220S} to MN-α2-GST was more profound in *naa20*Δ *ubr1*Δ *doa10*Δ cells (bearing Nt-unacetylated MN-α2-GST because of their lack of NatB Nt-acetylase) than *ubr1*Δ *doa10*Δ cells (bearing mostly Nt-acetylated MN-α2-GST but little, if any, Nt-unacetylated MN-α2-GST) (Fig. 2*I*). These results indicate that Ubr1 mediates degradation of Nt-unacetylated MN-α2-GST, whereas Doa10 targets Nt-acetylated AcMN-α2-GST (Fig. 2*J*) in agreement with our previous identification of Doa10 as an Ac/N-recognin (8).

Ubr1-dependent degradation of MN-α2-GST or MQ-α2-GST requires Ate1 and Nta1

Nt-sequence analysis using Edman degradation revealed that MN-α2-GST purified from *naa20*Δ *ubr1*Δ *doa10*Δ cells contained mixtures of ~64% Arg–Asp–Lys–Ile–Pro (RDKIP) and ~36% DNA-encoded Met–Asn–Lys–Ile–Pro (MNKIP) (Fig. 3*A*). Thus, we presumed that the detected RD-α2-GST in *naa20*Δ *ubr1*Δ *doa10*Δ cells arose from NME, followed by Nt-deamidation and subsequent Nt-arginylation in compliance with the previously well-established hierarchy of the Arg/N-end rule pathway (Fig. S1*A*). Indeed, CHX-chases showed that Nt-unacetylated MN-α2-GST in *naa20*Δ cells was virtually completely stabilized by the absence of either Ate1 or Nta1 (Fig. 3, *D–G*).

We next examined, in *naa20*Δ cells, the degradation of MZ-α2-GSTs that were otherwise identical but had different residues at position 2 (Z = Asn, Gln, Asp, Glu, Lys). Among these, MN-α2-GST ($t_{½}$ ≈23 min) and MQ-α2-GST ($t_{½}$ ≈20 min) were markedly short-lived in contrast to the relatively long-lived MD-α2-GST ($t_{½}$ ≈35 min), ME-α2-GST ($t_{½}$ ≈50 min), or MK-α2-GST ($t_{½}$ ≈53 min) (Fig. 3, *B* and *C*). Moreover, the short-lived MQ-α2-GST of *naa20*Δ cells was also greatly stabilized by the absence of either Nta1 or Ate1 (Fig. 3, *F* and *G*), as was MN-α2-GST (Fig. 3, *D* and *E*), indicating that the MQ-starting reporters also necessitate Nt-deamidation and subsequent Nt-arginylation prior to their Ubr1-mediated degradation.

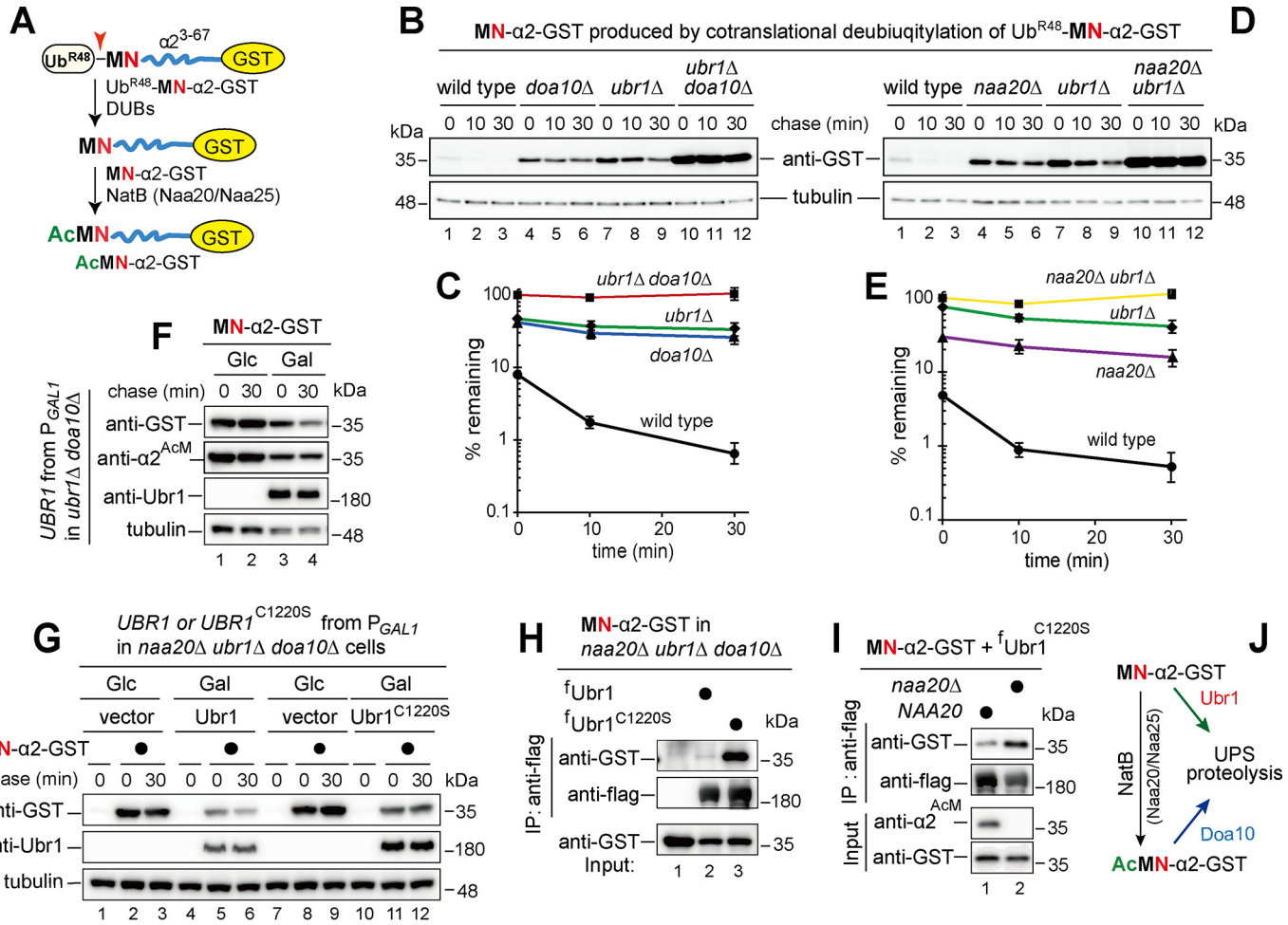

Figure 2. Ubr1 mediates degradation of Nt-unacetylated MN-α2-GST. *A,* co-translational deubiquitylation of Ub^{R48}-MN-α2-GST produces MN-α2-GST *in vivo*. The resulting MN-α2-GST is Nt-acetylated by NatB complex. *B,* CHX chases of MN-α2-GST in WT, *doa10Δ*, *ubr1Δ*, and *ubr1Δ doa10Δ S. cerevisiae* for 0, 10, and 30 min. *C,* quantitation of data in *B*. *D,* same as in *B,* but with WT, *naa20Δ*, *ubr1Δ*, and *naa20Δ ubr1Δ S. cerevisiae*. *E,* quantitation of data in *D*. The *graphs* in *C* and *E* show quantitation of data as mean ± S.D. from three independent experiments. *F,* same as in *B* but for 0 and 30 min in *ubr1Δ doa10Δ* cells expressing ^{f}Ubr1 from the P_{GAL1} promoter. The yeast cells were grown at 30 °C to A_{600} = ~0.8 in SRaf medium, followed by the addition of either galactose (for *UBR1* induction) or glucose (for *UBR1* repression). *G,* same as in *F* but in *naa20Δ ubr1Δ doa10Δ* cells expressing vector only, ^{f}Ubr1, or catalytically inactive mutant ^{f}Ubr1^{C1220S}. *H,* extracts of *naa20Δ ubr1Δ doa10Δ* cells expressing MN-α2-GST and ^{f}Ubr1 or ^{f}Ubr1^{C1220S} were subject to immunoprecipitation with anti-FLAG–agarose. The bound proteins were analyzed via SDS-PAGE and immunoblotting with anti-GST or anti-FLAG antibodies. The *bottom panel* shows the 1% input that was used for immunoprecipitation. *I,* same as in *H* but extracts of *NAA20* or *naa20Δ S. cerevisiae* (*ubr1Δ doa10Δ*) cells expressing MN-α2-GST and ^{f}Ubr1^{C1220S}. *J,* co-targeting scheme of MN-α2-GST via the Ubr1- and NatB/Doa10-mediated degradation by the Ub-proteasome system (*UPS*).

MetAPs cleave the Nt-M of MN-α2-GST and MQ-α2-GST for degradation

S. cerevisiae contains two MetAPs (Map1 and Map2), which redundantly cut off the Nt-M of nascent proteins, but only if the residue at position 2 is no larger than Val (34). Nonetheless, given the evident involvement of Ubr1, Ate1, and Nta1 in the degradation of MN-α2-GST or MQ-α2-GST (Figs. 2 and 3), we presumed that MetAPs might process the Nt-M of the reporters before they are targeted by the Arg/N-end rule pathway (Fig. 4*A*). To test this possibility, we expressed MN-α2-GST or MQ-α2-GST from the P_{CUP1} promoter on a low-copy-number CEN plasmid in *map1Δ naa20Δ* cells in either the presence or absence of the specific Map2 inhibitor, fumagillin. Tellingly, short-lived MN-α2-GST and MQ-α2-GST were strongly stabilized in *map1Δ naa20Δ* cells by fumagillin-mediated Map2 inactivation (Fig. 4, *B* and *C*). Altogether, we conclude that MetAPs can noticeably cleave the Nt-M of proteins, even with tertiary destabilizing Asn or Gln present at position 2, thus triggering their degradation by the Arg/N-end rule pathway *in vivo* (Fig. 4*A*).

Arg/N-end rule pathway mediates degradation of human MN-TFG

The observation of the Arg/N-end rule-dependent degradation of MN-α2-GST and MQ-α2-GST (Fig. 4) post-NME prompted us to search for native MQ/MN-starting proteins that are targeted for degradation by the Arg/N-end rule pathway. Surprisingly (and unexpectedly), our independent yeast two-hybrid (Y2H) screen using a C-terminally truncated human $UBR1^{1-1031}$ fragment with the previously defined substrate-binding sites (35) repeatedly isolated a human tropomyosin–receptor kinase–fused gene (TFG) as its binding partner (Fig. 5, *A* and *C*). Interestingly, the screened TFG-harboring prey vectors retained a stop codon just upstream of *TFG ORF* (ORF) following the *GAD*-coding sequence (Fig. 5*A*); *GAD* encodes the Gal4 transcription–activation domain, and native

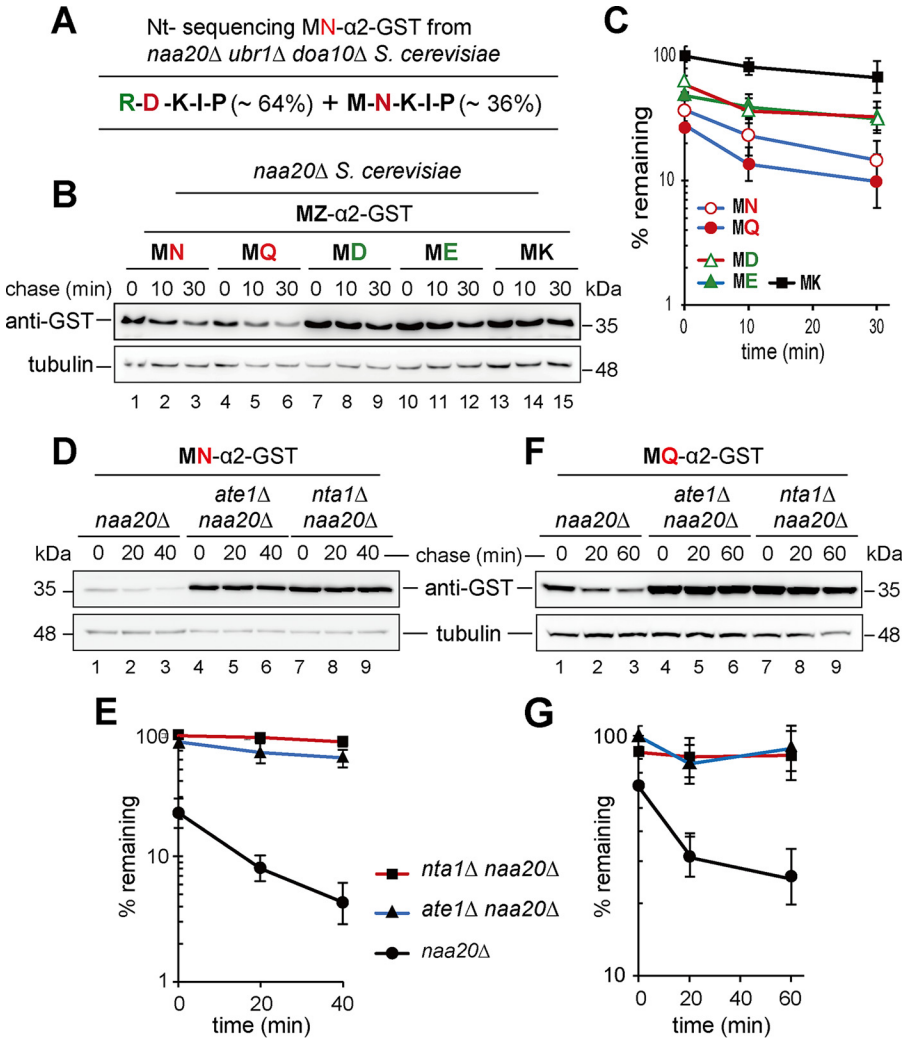

Figure 3. Degradation of Nt-unacetylated MN/MQ-α2-GSTs require Nta1, Ate1, and Ubr1. *A,* determination of the Nt sequences of MN-α2-GST purified from *naa20Δ ubr1Δ doa10Δ S. cerevisiae*. *B,* CHX chases of MZ-α2-GST for 0, 10, and 30 min in *naa20Δ S. cerevisiae*. Z = Asn, Gln, Asp, Glu, or Lys. *C,* Quantitation of Data in *B*. *D,* same as in *B* but with MN-α2-GST for 0, 20, and 40 min in *naa20Δ*, *ate1Δ naa20Δ*, or *nta1Δ naa20 Δ S. cerevisiae*. *E,* quantitation of data in *D*. *F,* same as in *D* but for 0, 20, and 60 min with MQ-α2-GST. *G,* Quantitation of Data in *F*. The *graphs* show quantitation of data as mean ± S.D. of three independent experiments.

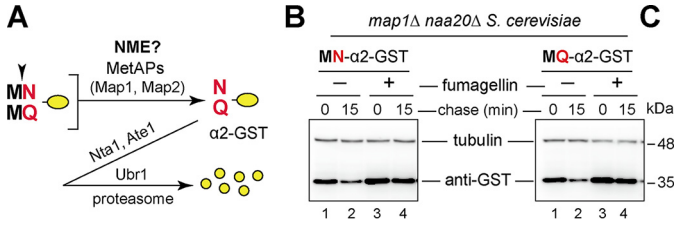

Figure 4. MetAPs create the tertiary N-degrons of the Arg/N-end rule pathway. *A,* parsimonious scheme of the NME-mediated degradation of MN-α2-GST and MQ-α2-GST. *B,* CHX chases of MN-α2-GST in *map1Δ naa20Δ S. cerevisiae* for 0 and 15 min in either the presence or absence of a Map2 inhibitor fumagillin (final amount, 5 μg/ml). *C,* same as in *B* but with MQ-α2-GST.

TFG ORF comprises an MN N terminus and an intrinsic transcription-activation domain (36). Hence, we postulated that the resulting MN-TFG would activate the expression of the Y2H reporters through a direct interaction with the Gal4-binding domain–UBR1$^{1-1031}$ fusion, even in situations lacking N-terminally positioned GAD (Fig. 5, *A* and *C*). To verify this possibility, we further mapped the TFG-binding site of UBR1 by repeating the Y2H assays using the truncated UBR1 derivatives as baits and found that TFG bound to the UBR box (type 1 site)– containing UBR1$^{1-1031}$, UBR1$^{1-632}$, UBR1$^{1-191}$, UBR1$^{93-221}$, or UBR1$^{93-191}$, but not to the UBR box lacking UBR1$^{93-157}$ and UBR1$^{167-1031}$ (Fig. 5, *B* and *C*). The identical MN-starting sequences of MN-TFG and MN-α2-GST suggested that MN-TFG would be subject to NME, followed by Nt-deamidation and subsequent Nt-arginylation before its targeting by UBR1. Indeed, loss of either Nta1 or Ate1 almost completely abrogated the binding of UBR1 to MN-TFG in Y2H assays (Fig. 5*D*).

Given these results, we sought to examine further whether the Arg/N-end rule pathway mediated the degradation of MN-TFG in mammalian cells by expressing the C-terminal triply FLAG-tagged human MN-TFG (MN-TFG$_{f3}$) in *Ate1*$^{+/+}$ WT mouse fibroblast (MEF) cells and *Ate1*$^{-/-}$ knockout (KO) MEF cells. Upon CHX chases, MN-TFG$_{f3}$ became short-lived in WT *Ate1*$^{+/+}$ MEF cells, but greatly stabilized in *Ate1*$^{-/-}$ KO MEF cells (Fig. 5, *E* and *F*), despite almost no significant changes in the levels of *TFG$_{f3}$* mRNA between *Ate1*$^{+/+}$ WT MEF cells and *Ate1*$^{-/-}$ KO MEF cells (Fig. 5*G*). Therefore, the observed strong augmentation of the MN-TFG$_{f3}$ level in *Ate1*$^{-/-}$ KO

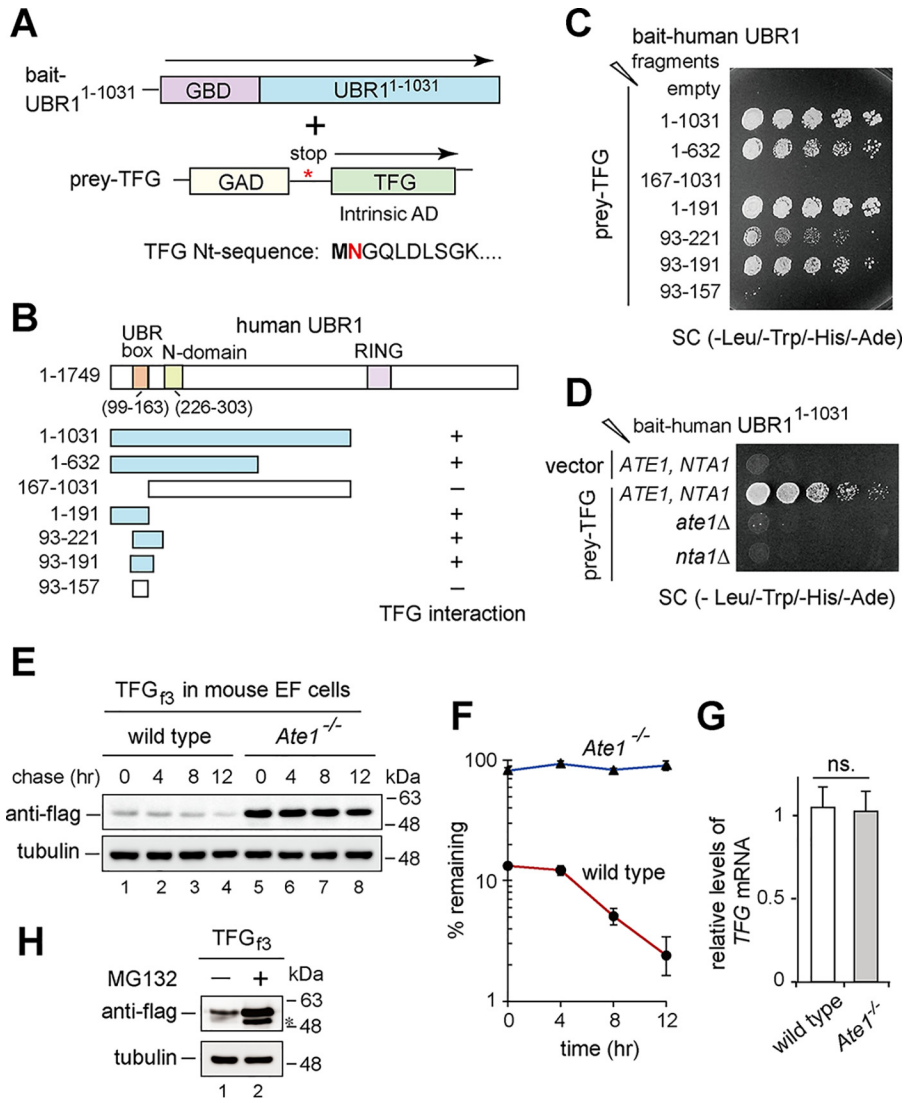

Figure 5. Human MN-TFG is degraded by the Arg/N-end rule pathway. *A,* schematic representation of human *UBR1*$^{1-1031}$ in Y2H bait vector and human *TFG* in Y2H prey vectors to be screened. *B,* UBR box, the N-domain and the RING domain of human UBR1. Fragments of UBR1 used to map its TFG-binding region are depicted *below* the diagram. *C,* interaction of TFG with UBR1 fragments upon Y2H assays. *D, in vivo* detection of UBR1$^{1-1031}$–TFG interactions in *ATE1 NTA1*, *ate1*Δ, and *nta1*Δ *S. cerevisiae* using Y2H assay. *S. cerevisiae* cells co-expressing bait and prey plasmids were serially diluted 5-fold and spotted on SC (−Leu/Trp) or SC(−Leu/Trp/His/Ade) plates (see "Experimental procedures" for details). *E,* CHX chases of C-terminal triply FLAG-tagged human TFG (TFG_{f3}) in *Ate1*$^{+/+}$ WT and *Ate1*$^{-/-}$ KO MEF cells for 0, 4, 8, and 12 h. *F, graph* represents quantitation of data in *E* with mean ± S.D. of three independent experiments. *G,* relative levels of human *TFG*$_{f3}$ mRNAs in WT and *Ate1*$^{-/-}$ KO MEF cells using RT-qPCR. The data presented are mean ± S.D. in triplicate for each sample. *H,* steady-state levels of TFG_{f3} in HeLa cells with or without the proteasome inhibitor MG132.

MEF cells most likely arises from alterations in the rate of its initial proteolytic decay (especially in accordance with many previous supporting studies) for the substantial co-translational degradation of nascent proteins (37–39). Of note, the degradation of MN-TFG_{f3} also requires the 26S proteasome because the steady-state level of MN-TFG_{f3} is greatly up-regulated by the presence of the proteasome inhibitor MG-132 (Fig. 5*H*). Overall, these results suggest that MN-TFG_{f3} would be degraded by the Arg/N-end rule pathway involving consecutive reactions of NME, Nt-deamidation, as well as subsequent Nt-arginylation in mammalian cells.

Arg/N-end rule pathway mediates degradation of S. cerevisiae MQ-Rad16

The positive Y2H interaction of the human UBR box with Nt-arginylated TFG bearing an intrinsic transcription activation domain (without GAD) (Fig. 5, *B* and *C*) prompted us to search for Nt-arginylated proteins in *S. cerevisiae*, in which ~9% of DNA-encoded proteins contain an MQ/MN-starting N terminus according to the Saccharomyces Genome Database (https://www.yeastgenome.org/). To this end, we repeated the Y2H screen using a human UBR1$^{93-151}$ containing only a UBR box (type-1 binding) site as a bait and a yeast genomic DNA library (as preys) in the *ubr1*Δ Y2H strain, in which Nt-arginylated substrates are long-lived because of the ablation of Ubr1, the sole N-recognin of the Arg/N-end rule pathway. The resulting Y2H screen identified Rad16, a 91-kDa nucleotide excision repair protein (denoted MQ-Rad16 hereafter because it starts with an MQ N terminus). MQ-Rad16 also contains its own intrinsic transcriptional activation domain (40). Remarkably, and in agreement with the above observations with MN-TFG (Fig. 5, *A–D*), the interaction between human UBR1$^{93-151}$ and

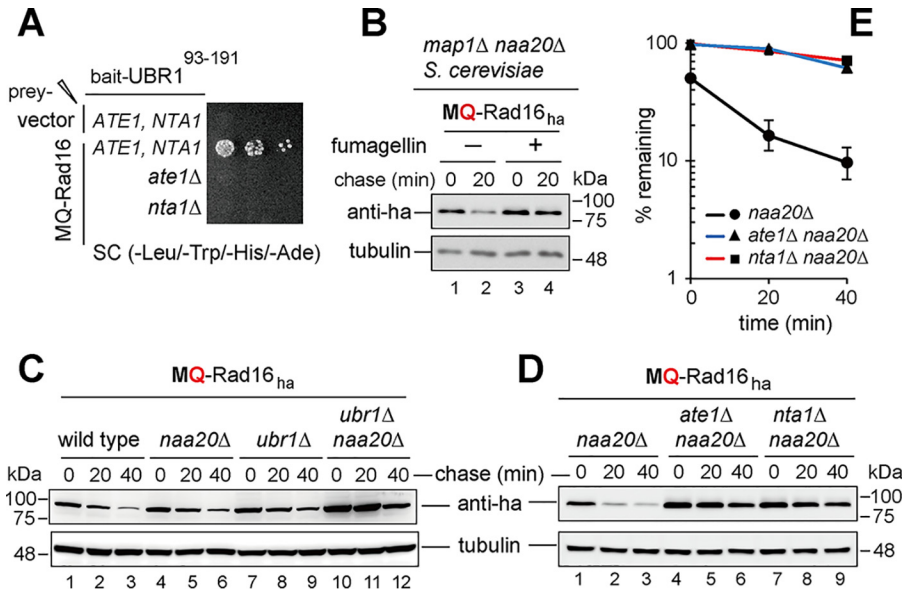

Figure 6. MQ-Rad16 is degraded by the Arg/N-end rule pathway. *A, in vivo* detection of human UBR1$^{93-191}$–MQ-Rad16 interaction in *ATE1 NTA1, ate1*Δ, or *nta1*Δ *S. cerevisiae* (*ubr1*Δ) using the Y2H assay. *B,* CHX chases of MQ-Rad16$_{ha}$ in *map1*Δ *naa20*Δ *S. cerevisiae* for 0 and 20 min in either the presence or absence of fumagillin (final amount, 5 μg/ml). *C,* CHX chases of MQ-Rad16$_{ha}$, for 0, 20, and 40 min, in WT, *naa20*Δ, *ubr1*Δ, or *ubr1*Δ *naa20*Δ *S. cerevisiae*. *D,* same as in *C* but in *naa20*Δ, *ate1*Δ *naa20*Δ, or *nta1*Δ *naa20*Δ *S. cerevisiae*. *E, graph* shows quantitation of data in *D* as mean ± S.D. of three independent experiments.

MQ-Rad16 was abolished by the loss of either Ate1 or Nta1 upon Y2H assays (Fig. 6*A*).

Consistent with the results observed for MN-α2-GST and MQ-α2-GST (see Fig. 4 for details), fumagillin-mediated inactivation of Map2 also caused a discernible stabilization of C-terminally ha-tagged MQ-Rad16 (MQ-Rad16$_{ha}$) in *map1*Δ *naa20*Δ cells (Fig. 6*B*), indicating the involvement of NME in the degradation of MQ-Rad16$_{ha}$ in *S. cerevisiae*. Moreover, CHX chases showed that MQ-Rad16$_{ha}$ was short-lived in WT cells, but partially stabilized in both single-mutant *naa20*Δ cells or *ubr1*Δ cells (Fig. 6*C*). MQ-Rad16$_{ha}$ was more stabilized in double-mutant *naa20*Δ *ubr1*Δ cells (Fig. 6*C*). Furthermore, MQ-Rad16$_{ha}$ was also long-lived in *ate1*Δ *naa20*Δ cells or *nta1*Δ *naa20*Δ cells (Fig. 6, *D* and *E*), indicating that MQ-Rad16$_{ha}$ was preliminarily processed via NME, Nt-deamidation, and subsequent Nt-arginylation before the targeting of the protein by Ubr1 (Fig. 6).

Ablation of the Arg/N-end rule pathway ameliorates the growth defect of naa20Δ cells at 37 °C

Given that Nt-acetylation competitively inhibits not only the activity of MetAPs, but also the recognition of substrate proteins by Ubr1 (5, 6), we presumed that the loss of NatB (Naa20) Nt-acetylase would trigger the NME-mediated degradation of a vast range of MN/MQ-starting proteins via the Arg/N-end rule pathway, thus increasing the susceptibility of yeast cells to specific stresses. Indeed, the growth of *naa20*Δ *S. cerevisiae* is hypersensitive to pleiotropic stressors, including heat, salts, drugs, ultraviolet light, etc. (41). Strikingly, we observed that the absence of Nta1 substantially rescued the defective growth of *naa20*Δ cells at 37 °C (Fig. 7*A*). Moreover, the lack of either Ate1 or Ubr1 more profoundly suppressed the defective growth of *naa20*Δ cells at 37 °C than that of Nta1 (Fig. 7*A*), suggesting the possibility that NME may also cause degradation of MD/ME-starting proteins, which bypass Nta1 for degradation via the Arg/N-end rule pathway. Indeed, this is in agreement with our recent observation that degradation of some reporters starting with the MD N terminus requires Ubr1 in *naa20*Δ cells (12). Collectively, these results indicate that the previously unexplained slow-growth phenotype of *naa20*Δ cells at 37 °C (41) may arise, in part, from low levels of Nt-unacetylated MN/MQ-starting proteins because of their vulnerable degradation at higher temperatures via the Arg/N-end rule pathway (Fig. 7*B*).

Discussion

Because of the strong processing activity of MetAPs toward Nt-M bearing small residues at position 2, NME is assumed to yield only stabilizing Nt-residues (Nt-G, -A, -S, -C, -T, -V, or -P) of the Arg/N-end rule pathway in *S. cerevisiae* (1, 9). As opposed to the typical substrate specificities of MetAPs, this study shows that MetAPs can produce the tertiary destabilizing residues Asn or Gly of the Arg/N-end rule pathway by removing the Nt-M of native proteins (MQ-Rad16 and MN-TFG) and model substrates *in vivo* (MN-α2-e^{K}-ha-Ura3, MN-α2-GST, and MQ-α2-GST) (Figs. 1–6).

In line with our present findings, global proteomic analyses bear out that the Asn or Gln at the 2nd position in some native proteins is exposed to the N terminus without the retention of the initiator Met (42). Additionally, *S. cerevisiae* Map1 processes, to an inefficient but significant extent, the Nt-M of a synthetic peptide with a MN N terminus *in vitro* (43, 44). Knop and co-workers (45) also reported, using multiplexed protein stability profiling for the quantitative and systematic mapping of degrons in the yeast Nt-proteome, that 10 MN-starting reporters and an Nt-truncated isoform of the mannosyltransferase MN-Ktr2 (with Met–Asn N terminus) may involve Map1-mediated NME for the Arg/N-end rule pathway.

Strikingly, Varshavsky and co-workers (46) first identified the engineered reporter Met–Gln–Leu–Ser–Ile–Ile–Asp–

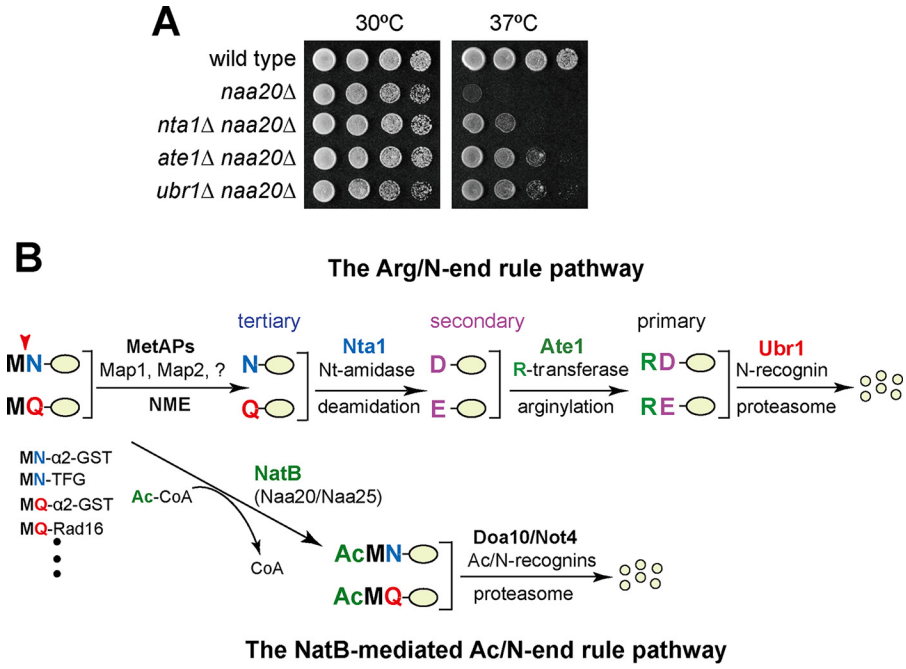

Figure 7. Interplay between the Arg/N-end rule and the NatB-mediated Ac/N-end rule pathway. *A,* growth of WT, *naa20*Δ, *ate1*Δ *naa20*Δ, *nta1*Δ *naa20*Δ, or *ubr1*Δ *naa20*Δ *S. cerevisiae*. Equal amounts of indicated cells were 5-fold serially diluted and spotted on YPD plates. The plates were incubated at 30 or 37 °C for 3 days. *B,* diagram representing the functional and mechanical cooperation between the Arg/N-end rule and the NatB-mediated Ac/N-end rule pathways. The Ac/N-end rule pathway directly targets Nt-acetyl tag of Nt-acetylated AcMN/AcMQ-starting proteins. However, Nt-unmodified but otherwise identical MN/MQ-starting proteins are vulnerable to NME and thereby degraded by the cascades of the Arg/N-end rule pathway.

Pro–Asp–Gly–Thr (MQLSIIDPDGT)-e^{K}-ha-Ura3 (23Q-Ura3) with Gln at position 2, whose degradation requires Nta1, Ate1, and Ubr1. However, the absence of either Map1 or Map2 does not significantly affect the degradation of 23Q-Ura3, suggesting the overlapping action of MetAPs or unknown dedicated aminopeptidases (46). Furthermore, Finley and co-workers (47) isolated an MH-starting PB12 reporter that undergoes NME, thereby exposing the penultimate His (a primary destabilizing residue of the Arg/N-end rule pathway) at its N terminus. Of note, the Ubr1-mediated degradation of the PB12 reporter is also unaffected in *map1*Δ cells. Therefore, the possibility cannot be excluded that not only MetAPs but also as yet unknown aminopeptidases can participate in the NME of MN/MQ-starting proteins according to their Nt-sequence context or structural conformation.

The present study overtly reveals NME as another critical process of the Arg/N-end rule pathway in the creation of tertiary destabilizing residues by demonstrating that Ubr1-mediated recognition of MN/MQ-starting proteins necessitates consecutive reactions of NME, Nt-deamidation, and subsequent Nt-arginylation (Figs. 2–6 and 7*B*). Accordingly, the resulting NME enormously increases the number of Arg/N-end rule substrates, considering that MN/MQ-starting proteins encompass about 9% of all nuclear DNA-encoded proteins. Nonetheless, it should be noted that the previously overlooked or underestimated requirement of NME in the degradation of MN/MQ-starting substrates by the Arg/N-end rule pathway most likely stems from two redundant (overlapping) MetAPs (Map1 and Map2) and the alternative proteolytic route by the Ac/N-end rule pathway, because the ablation effects of either single MetAP or the Arg/N-end rule pathway can be efficiently suppressed by the other MetAP or the Ac/N-end rule pathway, respectively.

Notably, Nt-acetylation confers the opposite impacts on protein stability, particularly because it not only creates Ac/N-degrons of the Ac/N-end rule pathway, but also concomitantly precludes the destruction of proteins by the Arg/N-end rule pathway (6, 7, 9). Hence, many MN/MQ-starting proteins are susceptible to the NME-mediated Arg/N-end rule pathway, and also, alternatively, to the Ac/N-end rule pathway through their Nt-acetylated Met, as demonstrated in the degradation patterns of MN-α2-e^{K}-ha-Ura3, MN-α2-GST, MQ-α2-GST, or MQ-Rad16$_{ha}$ (Figs. 1–3 and 6).

In addition and analogous to our previous finding that Nt-acetylation transforms an MΦ (a hydrophobic residue)/N-degron into an AcMΦ/N-degron, thus switching the targeting route of an MΦ-starting protein to the Ac/N-end rule pathway (Fig. S1*C*) (6, 13, 48), the NatB-mediated Nt-acetylation of MN/MQ-starting proteins would not only preclude their NME-mediated degradation by the Arg/N-end rule pathway, but also provoke their alternative proteolytic route via the Ac/N-end rule pathway. Consequently, dual or alternative targeting of MN/MQ-starting proteins by both the Arg/N-end rule pathway and the NatB-mediated Ac/N-end rule pathway would degrade these proteins cooperatively, irrespective of their Nt-acetylation states (Fig. 7*B*). Indeed and in a similar outcome to that of MΦ/N-degron–containing proteins (13), MN/MQ-starting proteins, such as MN-α2-GST, MQ-α2-GST, and MQ-Rad16$_{ha}$, were more strongly stabilized in the double mutant *ubr1*Δ *naa20*Δ cells than in the single mutant *ubr1*Δ or *naa20*Δ cells (Figs. 2, 3, and 6), indicating the co-targeting of MN/MQ-starting substrates by the Arg/N-end rule

and the NatB-mediated Ac/N-end rule pathways. However, the actual targeting mechanism of MN/MQ-starting proteins by Ubr1 is substantially different from that of MΦ-starting proteins. In particular, Ubr1 recognizes MN/MQ-starting proteins after their preliminary modifications (consisting of NME, Nt-deamidation, and subsequent Nt-arginylation) in contrast to its direct binding to the nonacetylated Nt-M of MΦ-starting proteins (Fig. 7*B*) (6, 13, 48).

It is also noteworthy that Nt-acetylation also modulates the activities of E3 Ub ligases, 26S proteasomes, and molecular chaperones (6). Furthermore, the antagonistic (triggering and restraining) impacts of Nt-acetylation on the Arg/N-end rule and the Ac/N-end rule pathways, respectively, increase the complexities of intracellular protein degradation more profoundly than those previously assumed, thereby making it particularly difficult to identify or predict the specific proteolytic pathway of a given protein using specific genetic studies harnessing a single gene deletion or knockdown, etc. (6, 7, 48).

Deg1 represents the first 67 residues of Matα2 (49). In this study, we also demonstrated here that MN-α2-GST (Deg1-GST) was significantly and substantially stabilized in *naa20*Δ cells that lacked a catalytic subunit of NatB Nt-acetylase (Fig. 2*B*) in agreement with previous observations of MN-α2-e^K-ha-Ura3 (Deg1-e^K-ha-Ura3) and MN-α2-Leu2$^{M1\Delta}$ (another Deg1 fusion protein) (8, 50). Conversely, it is also reported that the loss of Naa20 very weakly affects the degradation of endogenous Matα2, as well as other Deg1 fusions such as MN-α2-FLAG-Ura3 (Deg1-FLAG-Ura3) (49). The cited study interpreted these results as an indication that Nt-acetylation has little effect on the recognition of Doa10 for its substrates (49), in contrast to our previous finding that Doa10 works as an Ac/N-recognin (8). Although these discrepancies in the Nt-acetylation–dependent degradation of Deg1 fusions remain to be further examined, we infer that the shifting rate or extent of the NatB-mediated Ac/N-end rule pathway to the NME-mediated Arg/N-end rule pathway may cause distinct proteolytic outcomes, particularly according to the sequence context of Deg1 substrates or *naa20*Δ strains that are used in our studies and those of others (8, 49, 50).

Strikingly, and with conceptual similarity to the results with *naa20*Δ cells, *dfm1*Δ cells (lacking the rhomboid derlin Dfm1) are reported to have very dissimilar proteolytic patterns (51). For instance, some studies do not detect any defects in the degradation of ER-associated protein degradation (ERAD) substrates in *dfm1*Δ cells (52, 53), whereas others reveal the significant stabilization of a subset of ERAD substrates in the absence of Dfm1 (54, 55). More recently, Hampton and co-workers (51) resolved the controversial role of Dfm1 in ERAD by demonstrating that *dfm1*Δ cells rapidly assume suppression and thereby compromise ERAD by up-regulating the alternative proteolytic pathway.

Likewise, in *naa20*Δ cells, the ablation of the NatB-mediated Ac/N-end rule pathway would rapidly trigger the other NME/NatB-mediated Arg/N-end rule pathway, thus exhibiting the observed comparable degradation of Deg1 fusions in both WT cells and *naa20*Δ cells (49), which remains to be tested. Furthermore, our most recent genetic and biochemical experiments reveal that TEB4 (a mammalian homolog of Doa10) (23) more preferentially binds to Nt-acetylatable native proteins, such as RGS2 and PLIN2, than to their nonacetylatable counterparts, which is in agreement with our previous identification of TEB4 (Doa10) as an Ac/N-recognin (26).

This study also demonstrates that human TFG is a substrate of the NME-mediated Arg/N-end rule pathway. Endogenous TFG is involved in the spatial coordination of the early secretory event from endoplasmic reticulum to Golgi by binding to the coat protein complex II (COPII) (56).

Remarkably, the *TFG* gene is frequently identified as a chromosomally translocated chimeric gene with many oncogenes, such as *NTRK1* (a neurotrophic receptor tyrosine kinase) in thyroid papillary carcinomas, *ALK* (anaplastic lymphoma kinase), *NOR1* (a nuclear orphan receptor), *NEMO* (NF-κB essential modulator), *TANK* (TRAF-associated NF-κB activator), *TEC* (translocated in extraskeletal genes in some cancer cells), etc. (36, 57–59). Interestingly, the resulting TFG-fusion oncogenic proteins contain TFG primarily at their N-terminal region. Therefore, the present finding that the MetAPs-mediated Arg/N-end rule pathway degrades MN-TFG suggests that the N-terminal TFG of these oncogenic fusion proteins would act as a portable degron for the NME-mediated Arg/N-end rule pathway. As a result, the TFG-mediated dysregulation of oncogenic proteins most likely promotes tumorigenesis. Elucidating whether Nt-fused TFG can trigger the degradation of oncogenic fusion proteins via the MetAPs-mediated Arg/N-end rule pathway in malignant cancer cells is therefore of great interest.

Experimental procedures

Miscellaneous reagents and antibodies

Cycloheximide (C7698), yeast protease inhibitor mixture (P8215), phenylmethylsulfonyl fluoride (93482), and fumagillin (F6771) were purchased from Sigma. Chicken egg white lysozyme (LDB0308) was purchased from Bio Basic (Markham, Ontario, Canada), and MG-132 (474790) was from Calbiochem. Anti-FLAG M2 (F1804), anti-ha (H9658), and anti-tubulin (T5168) antibodies were purchased from Sigma. Anti-GST (A00865) antibodies were sourced from GenScript (Piscataway, NJ). Secondary antibodies for immunoblotting were horseradish peroxidase–conjugated goat anti-rabbit (170-6515, Bio-Rad) or anti-mouse (170-6516, Bio-Rad) antibodies, with detection using Clarity Western ECL substrate (170-5061, Bio-Rad), according to the manufacturer's instructions. Dynabeads protein A and G (10001D and 10003D, ThermoFisher Scientific, Waltham, MA) and GSH-Sepharose 4B (17-0756-05, GE Healthcare) were used for co-immunoprecipitation and pulldown assays.

Yeast strains, culture media, and genetic methods

S. cerevisiae strains used in this study are described in Table 1. Strain construction and transformation were conducted using standard techniques (60). *S. cerevisiae* CHY367, CHY368, CHY860, CHY907, CHY908, CHY2009, CHY2014, CHY1015, CHY2016, CHY2017, CHY3129, CHY3186, CHY5052, CHY5091, CHY5092, CHY5093, CHY5094, and CHY5141 were constructed through the PCR-mediated gene disruption method using pFA6a-KanMX6, pFA6a-HphNT1, or pFA6a-NatNT2 modules. *S. cerevisiae* cells were cultured in YPD (1%

Table 1
***S. cerevisiae* strains used in this study**

Strains	Relevant genotypes	Sources
JD52	*MAT***a** *trp1-63 ura3-52 his3-200 leu2-3112, lys2-801*	Lab collection
JD53	*MATα trp1-63 ura3-52 his3-200 leu2-3112, lys2-801*	Lab collection
JD83-1A	*ubr1Δ::HIS3* in JD53	Lab collection
BY4741	*MAT***a** *his3-1 leu2-0 ura3-0 met15-0*	Lab collection
BY4742	*MATα his3-1 leu2-0 ura3-0 can1-100*	Open Biosystems
pJ69-4A	*MAT***a** *leu2-3,112 ura3-52 trp1-901 his3-200 gal4Δ gal80Δ GAL-ADE2 lys2::GAL1-HIS3 met2::GAL7-LacZ*	Lab collection
SC295	*MATa ura3-52 leu2-3,112 regl-501 gal1 pep4-3*	Lab collection
CHY223	*doa10Δ::KanMX6* in JD53	8
CHY229	*ubr1Δ::HIS3 doa10Δ::KanMX6* in JD53	This study
CHY324	*map1Δ::KanMX6* in BY4742	Open Biosystems
CHY367	*naa20Δ::NatNT2* in JD53	8
CHY368	*naa20Δ::NatNT2 ubr1Δ::HIS3* in JD53	12
CHY860	*naa20Δ::HphNT1 map1Δ::KanMX6* in BY4742	This study
CHY868	*ubr1Δ::NatNT2* in pJA69-4A	This study
CHY907	*ate1Δ::HphNT1* in pJA69-4A	This study
CHY908	*nta1Δ::HphNT1* in pJA69-4A	This study
CHY2009	*naa20Δ::NatNT2 ubr1Δ::KanMX6* in JD53	12
CHY2011	*naa20Δ::NatNT2 ubr1Δ::HIS3 doa10Δ::KanMX6* in JD53	This study
CHY2014	*ate1Δ::HphNT1* in JD53	This study
CHY2015	*naa20Δ::NatNT2 ate1Δ::HphNT1* in JD53	This study
CHY2016	*nta1Δ::HphNT1* in JD53	This study
CHY2017	*naa20Δ::NatNT2 nta1Δ::HphNT1* in JD53	This study
CHY3129	*naa20Δ::NatNT2 ate1Δ::HphNT1* in pJA69-4A	This study
CHY3186	*ubr1Δ::KanMX6* in JD53	12
CHY5052	*ubr1Δ::NatNT2 cup9Δ::KanMX6* in pJ69-4A	This study
CHY5091	*ubr1Δ::NatNT2 in* pJA69-4A	This study
CHY5092	*nta1Δ::HphNT1 ubr1Δ::NatNT2 in* pJA69-4A	This study
CHY5093	*ate1Δ::HphNT1 ubr1Δ::NatNT2* in pJA69-4A	This study
CHY5094	*nta1Δ::HphNT1 ubr1Δ::NatNT2 cup9Δ::KanMX6* in pJ69-4A	This study
CHY5141	*ate1Δ::HphNT1 ubr1Δ::NatNT2 cup9Δ::KanMX6* in pJ69-4A	This study

yeast extract, 2% peptone, and 2% glucose), SC (0.17% yeast nitrogen base, 0.5% ammonium sulfate, 2% glucose, and specific compounds to support the cell growth of specific auxotrophic strains), SRaf (SC with 2% raffinose instead of 2% glucose), or SGal (SC with 2% galactose instead of 2% glucose) media.

Plasmid construction

Tables 2 and 3 describe the plasmids and oligomers used in this study. To construct the pCH1525 vector that expressed Ub^{R48}-MN-$\alpha2^{3-67}$-GST from the P_{CUP1} promoter on a low-copy-number pRS314 vector, the *MN-α2*$^{3-67}$ and *GST* genes were PCR-amplified from pCH535 and pEG-KG using primer pairs OCH817/OCH992 and OCH613/OCH614. The resulting PCR products were digested with SacII/EcoRI and EcoRI/XhoI, respectively, and then triply ligated into SacII/XhoI-cut pCH535.

To construct pCH1591 that expressed human $UBR1^{1-1031}$ from a Y2H expression bait vector, human *UBR1*$^{1-1031}$ DNA was PCR-amplified from pCH432 carrying human *UBR1* cDNA using the primers OCH5001/OCH5003, digested with SfiI/SalI, and then cloned into SfiI/SalI-cut pGBKT7. To create pCH5003 that expressed TFG_{f3}, the human *TFG* gene was PCR-amplified from pCH5131, which was derived from the Y2H screen, using the primer pair OCH5017/OCH5018. The resulting PCR fragment was digested with BamHI/XbaI and inserted into BamHI/XbaI-cut pcDNA3.1(+). To construct pCH5054 that expressed MQ-$Rad16_{ha}$ from P_{CUP1} promoter on a low-copy-number pRS316 vector, *RAD16* was PCR-amplified from yeast genomic DNA using the primer pair OCH5067/OCH5069, digested with SpeI/SacI, and then ligated into SpeII/SacI-cut pCH692.

Table 2
Plasmids used in this study

Plasmids	Descriptions	Sources
pRS314	A CEN-based vector with a TRP marker	Lab collection
pRS316	A CEN-based vector with a URA marker	Lab collection
pRS425	2μ-based vector with a Leu marker	Lab collection
pGBKT7	A bait Y2H vector	Clontech
pACT2	A prey Y2H vector	Clontech
YEplac181	2μ-based vector with a *LEU2* marker	Lab collection
pEG-KG	*GST* from $P_{GAL1/10}$ in 2μ, *URA3* and *leu2-d* vector	Lab collection
pBAM	Ub-MH-e^K-ha-Ura3 in p314CUP1	Lab collection
pCH432	Human UBR1 cDNA in pCR-XL-TOPO	Open Biosystems
pCH473	pBAM derivative without *Sac*II site	Lab collection
pCH535	Ub^{R48}-MN-$\alpha2^{3-67}$-e^K-ha-Ura3 in p314CUP1	8
pCH692	p316CUP1	Lab collection
pCH1220	p424GAL1,10	Lab collection
pCH1525	Ub^{R48}-MN-$\alpha2^{3-67}$-GST in p314CUP1	This study
pCH1527	Ub^{R48}-MN-$\alpha2^{3-67}$-GST in p314CUP1	This study
pCH1531	Human TFG in pACT2	This study
pCH1591	Human $UBR1^{1-1031}$ in pGBKT7	This study
pCH1596	Human $UBR1^{167-1031}$ in pGBKT7	This study
pCH1633	^{f}Ubr1 in p425GAL	Lab collection
pCH1634	$^f Ubr1^{C1220S}$ in p425GAL	Lab collection
pCH1703	Ub^{R48}-MQ-$\alpha2^{3-67}$-GST in p314CUP1	This study
pCH1704	Ub^{R48}-MD-$\alpha2^{3-67}$-GST in p314CUP1	This study
pCH1705	Ub^{R48}-ME-$\alpha2^{3-67}$-GST in p314CUP1	This study
pCH5003	Human TFG_{f3} in pcDNA3.1 (+)	This study
pCH5004	Human $UBR1^{1-191}$ in pGBKT7	This study
pCH5007	Human $UBR1^{93-157}$ in pGBKT7	This study
pCH5008	Human $UBR1^{93-191}$ in pGBKT7-	This study
pCH5009	Human $UBR1^{93-221}$ in pGBKT7	This study
pCH5054	MQ-$Rad16_{ha}$ in p316CUP1	This study

Construction details for other plasmids are available upon request. All constructed plasmids were verified via DNA sequencing.

CHX-chase assays of protein degradation

S. cerevisiae cells were cultured to a 600 nm absorbance value (A_{600}) of ≈1.0 in YPD or SC media at 30 °C and then treated with CHX (at a final concentration of 0.2 mg/ml). Cell samples (equivalent to 1 ml of cell suspension at an A_{600} of 1) were collected at the indicated times via centrifugation for 2 min at

Table 3
Examples of PCR oligomers used in this study

Name	Primer sequences
OCH613	5′-GGTGAATTCGGTGCTGGAGCAGGTGCTATGTCCCCTATAC TAGGT TATTGG-3′
OCH614	5′-GGTCTCGAGTCAACGCGGAACCAGATCCGATTT-3′
OCH817	5′-GCTCCGCGGTGGTATGAATAAAA TACCCATTAAAGAC-3′
OCH992	5′-AATGAATTCAATCTTACGGTTTTTGTTGGCCCT-3′
OCH5001	5′-TATGGCCATGGAGGCCATGGCGGACGAGGAGGCTGGA-3′
OCH5003	5′-CGCGTCGACCTGGCGATGTAGCCTAGCAGCTTC-3′
OCH5107	5′-CCCGGATCCATGAACGGACAGTTGGATCTAAGT-3′
OCH5108	5′-ACATCTAGATCGATAACCAGGTCCAGGTTGGGT-3′
OCH5067	5′-ACAACTAGTATGCAAGAAGGGGGCTTTATCCGT-3′
OCH5069	5′-CCCGAGCTCCTAAGCGTAATCTGGAACATCGTATGGGTAG CTAGCGTT ATTGAATAAGAACTGTAAATC-3′
OCH6874	5′-CTCAGCAGCCTCAACAGTATGG-3′
OCH6875	5′-GGCTGACCAGAAAAGGCAGG-3′
OCH8104	5′-CACTGTCGAGTCGCGTCCA-3′
OCH8105	5′-CCACGATGGAGGGGAATACAG-3′

11,200 × *g* and resuspended in 1 ml of 0.2 M NaOH for 20 min on ice, followed by centrifugation for 2 min at 11,200 × *g*. Pelleted cells were resuspended in 50 μl of HU buffer (8 M urea, 5% SDS, 1 mM EDTA, 0.1 M DTT, 0.005% bromphenol blue, 0.2 M Tris-HCl, pH 6.8) containing 1× protein inhibitor mixture (Sigma) and incubated for 10 min at 70 °C. After centrifugation for 5 min at 11,200 × *g*, 10 μl of the resulting supernatants were separated via Tris-glycine SDS-PAGE, followed by immunoblotting with anti-GST (1:2,000), anti-ha (1:2,000), or anti-tubulin (1:4,000) antibodies.

For the CHX-chase assays of TFG_{f3}, $Ate1^{+/+}$ WT MEF cells and $Ate1^{-/-}$ KO MEF cells were maintained in DMEM supplemented with 10% FBS and 1× streptomycin/penicillin in a 5% CO_2 incubator at 37 °C. On day 1, 1×10^5 cells were seeded into 12-well culture plates and then transfected with 0.5 μg of pCH5003 and 3 μl of polyethyleneimine (PEI) (1 mg/ml stock solution in water, pH 7.0). After transfecting for 48 h, cells were treated with CHX (the final amount, 100 μg/μl) before harvesting and lysing in RIPA buffer (89900, ThermoFisher Scientific) at the indicated time points. Cell lysates were incubated on ice for 30 min and centrifuged for 15 min at 4 °C with 15,000 × *g*. Supernatants were collected, and the protein concentration was measured using the Bradford assay (500001, Bio-Rad), before mixing with Laemmli sample buffer and separating using Tris-glycine SDS-10% PAGE. TFG_{f3} and tubulin were detected using immunoblotting with anti-tubulin and anti-FLAG antibodies. Quantification of the resulting immunoblotting data were conducted using ImageJ software (http://rsb.info.nih.gov/ij/index.html).

Y2H screening and binding assays

To screen human UBR1-binding proteins, a human pancreas cDNA library cloned into the prey pACT2 vector (638820, Clontech) was transformed into *S. cerevisiae* strain pJ69 l4A expressing a bait pCH1591 (expressing human $UBR1^{1-1031}$) using the lithium-acetate protocol (61). Out of 7.6×10^6 transformants, 64 colonies were selected on SC (−Trp/−Leu/−His/−Ade) plates after a 3-day incubation at 30 °C. The library plasmids were rescued from 63 positive clones, amplified in *E. coli*, and then identified using DNA sequencing. Among these, 20 colonies carried the human *TFG* gene in the prey pACT2 vector. To define the binding of $UBR1^{1-1031}$ or its fragments to MN-TFG using the Y2H assay, pJ69-4A, CHY868 (*ubr1*Δ), CHY907 (*ate1*Δ), and CHY908 (*nta1*Δ) *S. cerevisiae* cells were co-transformed with pCH1531 (MN-TFG) and either pGBKT7 or pCH1591 ($UBR1^{1-1031}$), pCH1596 ($UBR1^{167-1031}$), pCH5004 ($UBR1^{1-191}$), pCH5007 ($UBR1^{93-157}$), pCH5008 ($UBR1^{93-191}$), or pCH5009 ($UBR1^{93-221}$). The resulting transformants bearing bait and prey plasmids were grown up to $A_{600} \approx 1$, serially diluted 5-fold, spotted on SC(−Leu/Trp), SC(−Leu/Trp/His), or SC(−Leu/Trp/Ade/His) plates, and then incubated for 3 days at 30 °C.

Because $UBR1^{93-191}$ contains the UBR box (type-1– binding site) only, yeast proteins bearing type-1– destabilizing residues and a transcription activation domain were screened from CHY5052 (*ubr1*Δ) *S. cerevisiae* co-expressing the bait vector pCH5008 and the Y2H-genomic libraries, largely as described above. To dissect the binding of $UBR1^{93-191}$ to MQ-Rad16 using yeast-based two-hybrid– binding assays, pJ69-4A, CHY5052 (*ubr1*Δ), CHY5094 (*nta1*Δ *ubr1*Δ), or CHY5141 (*ate1*Δ *ubr1*Δ) *S. cerevisiae* cells were co-transformed with pCH5043 (MQ-Rad16) and either pGBKT7, pCH1591, or pCH5008. The transformants were analyzed as described above.

N-terminal protein sequencing by Edman degradation

Approximately 5 μg of MN-α2-GST protein partially purified from *naa20*Δ *ubr1*Δ *doa10*Δ cells was separated on a Tris-SDS-10% polyacrylamide gel at 80 V for 90 min in SDS-PAGE running buffer. After electrophoresis, the gel was equilibrated in CAPS transfer buffer (10% methanol, 10 mM CAPS, pH 11) for 10 min before electroblotting onto a PVDF membrane (Immobilon P^{SQ}, Millipore, Billerica, MA). Electroblotting was performed at 80 mA overnight at 4 °C. The PVDF membrane was washed in distilled water for 10 min, stained with Coomassie Blue R-250 (0.1% R-250 in 50% methanol) for 10 min, and then distained twice for 15 min in a destaining buffer (50% methanol, 10% acetic acid). The relevant protein band of MN-α2-GST was cut and analyzed by Edman degradation using a model 492 cLC procise protein micro-sequencer (Applied Biosystems, GmbH) at the Protein Sequencing Laboratory (Seoul, South Korea).

Total RNA extraction and real-time RT-qPCR

For extraction of total RNA, 1×10^5 $Ate1^{+/+}$ WT MEF cells or $Ate1^{-/-}$ KO MEF cells were seeded onto a 12-well plate in DMEM, 10% FBS plus streptomycin/penicillin on day 1, and then transfected with 0.5 μg of PCH5003 and 3 μl of PEI. After a 48-h incubation, total RNA was extracted using an RNeasy mini kit (74104, Qiagen, Germantown, MD), according to the manufacturer's protocol. Five hundred ng of total RNAs were converted into cDNA using a TOPscript™ cDNA synthesis kit (Enzynomics, EZ005S, South Korea) in 20-μl reactions. Ten ng of cDNA from each sample were used for quantitative real-time RT-qPCR using a StepOnePlus Real-Time System (ThermoFisher Scientific), and Power SYBR Green PCR primer pairs OCH6874/OCH6875 for human *TFG* and OCH8104/OCH8105 for *ACTB* (encoding β-actin) were designed using NCBI Primer-BLAST. The RT-qPCR cycles were as follows: 95 °C for 10 min, followed by 40 cycles of 95 °C for 15 s and

59 °C for 1 min. To calculate relative *TFG* expression, the $\Delta\Delta CT$ method was used.

Statistical analysis

To calculate significant differences (p values), two-tailed paired Student's t tests were used through Microsoft Excel 2016. A p value of <0.05 was considered statistically significant. All the values are presented as mean ± S.D.

Author contributions—K. T. N. and C.-S. H. data curation; K. T. N., J.-M. K., and S.-E. P. formal analysis; K. T. N., J.-M. K., and S.-E. P. investigation; K. T. N., J.-M. K., and S.-E. P. methodology; K. T. N. and C.-S. H. writing-original draft; C.-S. H. supervision; C.-S. H. funding acquisition; C.-S. H. project administration; C.-S. H. writing-review and editing.

Acknowledgments—We are grateful to Y.-T. Kwon (Seoul National University, South Korea) for providing Ate1$^{+/+}$ MEF cells and Ate1$^{-/-}$ MEF cells, and we also thank the current and former members of Hwang's laboratory for their assistance and comments on the paper.

References

1. Giglione, C., Fieulaine, S., and Meinnel, T. (2015) N-terminal protein modifications: bringing back into play the ribosome. *Biochimie* **114,** 134–146 CrossRef Medline
2. Arfin, S. M., and Bradshaw, R. A. (1988) Co-translational processing and protein turnover in eukaryotic cells. *Biochemistry* **27,** 7979–7984 CrossRef Medline
3. Frottin, F., Bienvenut, W. V., Bignon, J., Jacquet, E., Vaca Jacome, A. S., Van Dorsselaer, A., Cianferani, S., Carapito, C., Meinnel, T., and Giglione, C. (2016) MetAP1 and MetAP2 drive cell selectivity for a potent anticancer agent in synergy, by controlling glutathione redox state. *Oncotarget* **7,** 63306–63323 Medline
4. Ree, R., Varland, S., and Arnesen, T. (2018) Spotlight on protein N-terminal acetylation. *Exp. Mol. Med.* **50,** 90 CrossRef Medline
5. Van Damme, P., Hole, K., Gevaert, K., and Arnesen, T. (2015) N-terminal acetylome analysis reveals the specificity of Naa50 (Nat5) and suggests a kinetic competition between N-terminal acetyltransferases and methionine aminopeptidases. *Proteomics* **15,** 2436–2446 CrossRef Medline
6. Nguyen, K. T., Mun, S. H., Lee, C. S., and Hwang, C. S. (2018) Control of protein degradation by N-terminal acetylation and the N-end rule pathway. *Exp. Mol. Med.* **50,** 91 CrossRef Medline
7. Lee, K. E., Heo, J. E., Kim, J. M., and Hwang, C. S. (2016) N-terminal acetylation-targeted N-End rule proteolytic system: the Ac/N-End rule pathway. *Mol. Cells* **39,** 169–178 CrossRef Medline
8. Hwang, C. S., Shemorry, A., and Varshavsky, A. (2010) N-terminal acetylation of cellular proteins creates specific degradation signals. *Science* **327,** 973–977 CrossRef Medline
9. Varshavsky, A. (2011) The N-end rule pathway and regulation by proteolysis. *Protein Sci.* **20,** 1298–1345 CrossRef Medline
10. Cha-Molstad, H., Sung, K. S., Hwang, J., Kim, K. A., Yu, J. E., Yoo, Y. D., Jang, J. M., Han, D. H., Molstad, M., Kim, J. G., Lee, Y. J., Zakrzewska, A., Kim, S. H., Kim, S. T., Kim, S. Y., *et al.* (2015) Amino-terminal arginylation targets endoplasmic reticulum chaperone BiP for autophagy through p62 binding. *Nat. Cell Biol.* **17,** 917–929 CrossRef Medline
11. Chen, S. J., Wu, X., Wadas, B., Oh, J. H., and Varshavsky, A. (2017) An N-end rule pathway that recognizes proline and destroys gluconeogenic enzymes. *Science* **355,** eaal3655 CrossRef Medline
12. Kim, J. M., Seok, O. H., Ju, S., Heo, J. E., Yeom, J., Kim, D. S., Yoo, J. Y., Varshavsky, A., Lee, C., and Hwang, C. S. (2018) Formyl-methionine as an N-degron of a eukaryotic N-end rule pathway. *Science* **362,** eaa10174 CrossRef Medline
13. Kim, H. K., Kim, R. R., Oh, J. H., Cho, H., Varshavsky, A., and Hwang, C. S. (2014) The N-terminal methionine of cellular proteins as a degradation signal. *Cell* **156,** 158–169 CrossRef Medline
14. Hwang, C. S., Shemorry, A., Auerbach, D., and Varshavsky, A. (2010) The N-end rule pathway is mediated by a complex of the RING-type Ubr1 and HECT-type Ufd4 ubiquitin ligases. *Nat. Cell Biol.* **12,** 1177–1185 CrossRef Medline
15. Tasaki, T., Sriram, S. M., Park, K. S., and Kwon, Y. T. (2012) The N-end rule pathway. *Annu. Rev. Biochem.* **81,** 261–289 CrossRef Medline
16. Gibbs, D. J., Bacardit, J., Bachmair, A., and Holdsworth, M. J. (2014) The eukaryotic N-end rule pathway: conserved mechanisms and diverse functions. *Trends Cell Biol.* **24,** 603–611 CrossRef Medline
17. Dougan, D. A., Micevski, D., and Truscott, K. N. (2012) The N-end rule pathway: from recognition by N-recognins, to destruction by AAA+ proteases. *Biochim. Biophys. Acta* **1823,** 83–91 CrossRef Medline
18. Bachmair, A., Finley, D., and Varshavsky, A. (1986) *In vivo* half-life of a protein is a function of its amino-terminal residue. *Science* **234,** 179–186 CrossRef Medline
19. Dissmeyer, N., Rivas, S., and Graciet, E. (2018) Life and death of proteins after protease cleavage: protein degradation by the N-end rule pathway. *New Phytol.* **218,** 929–935 CrossRef Medline
20. Eldeeb, M., and Fahlman, R. (2016) The N-End rule: the beginning determines the end. *Protein Pept. Lett.* **23,** 343–348 CrossRef Medline
21. Lee, J. H., Jiang, Y., Kwon, Y. T., and Lee, M. J. (2015) Pharmacological modulation of the N-end rule pathway and its therapeutic implications. *Trends Pharmacol. Sci.* **36,** 782–797 CrossRef Medline
22. Shemorry, A., Hwang, C. S., and Varshavsky, A. (2013) Control of protein quality and stoichiometries by N-terminal acetylation and the N-end rule pathway. *Mol. Cell* **50,** 540–551 CrossRef Medline
23. Park, S. E., Kim, J. M., Seok, O. H., Cho, H., Wadas, B., Kim, S. Y., Varshavsky, A., and Hwang, C. S. (2015) Control of mammalian G protein signaling by N-terminal acetylation and the N-end rule pathway. *Science* **347,** 1249–1252 CrossRef Medline
24. Wadas, B., Borjigin, J., Huang, Z., Oh, J. H., Hwang, C. S., and Varshavsky, A. (2016) Degradation of serotonin *N*-acetyltransferase, a circadian regulator, by the N-end rule pathway. *J. Biol. Chem.* **291,** 17178–17196 CrossRef Medline
25. Xu, F., Huang, Y., Li, L., Gannon, P., Linster, E., Huber, M., Kapos, P., Bienvenut, W., Polevoda, B., Meinnel, T., Hell, R., Giglione, C., Zhang, Y., Wirtz, M., Chen, S., and Li, X. (2015) Two N-terminal acetyltransferases antagonistically regulate the stability of a nod-like receptor in *Arabidopsis*. *Plant Cell* **27,** 1547–1562 CrossRef Medline
26. Nguyen, K. T., Lee, C.-S., Mun, S.-H., Truong, N. T., Park, S. K., and Hwang, C. S. (2019) N-terminal acetylation and N-end rule pathway control degradation of the lipid droplet protein PLIN2. *J. Biol. Chem.* **294,** 379–388 CrossRef Medline
27. Dong, C., Zhang, H., Li, L., Tempel, W., Loppnau, P., and Min, J. (2018) Molecular basis of GID4-mediated recognition of degrons for the Pro/N-end rule pathway. *Nat. Chem. Biol.* **14,** 466–473 CrossRef Medline
28. Piatkov, K. I., Vu, T. T., Hwang, C. S., and Varshavsky, A. (2015) Formyl-methionine as a degradation signal at the N-termini of bacterial proteins. *Microb. Cell* **2,** 376–393 CrossRef Medline
29. Hu, R. G., Sheng, J., Qi, X., Xu, Z., Takahashi, T. T., and Varshavsky, A. (2005) The N-end rule pathway as a nitric oxide sensor controlling the levels of multiple regulators. *Nature* **437,** 981–986 CrossRef Medline
30. Lee, M. J., Tasaki, T., Moroi, K., An, J. Y., Kimura, S., Davydov, I. V., and Kwon, Y. T. (2005) RGS4 and RGS5 are *in vivo* substrates of the N-end rule pathway. *Proc. Natl. Acad. Sci. U.S.A.* **102,** 15030–15035 CrossRef Medline
31. Gibbs, D. J., Lee, S. C., Isa, N. M., Gramuglia, S., Fukao, T., Bassel, G. W., Correia, C. S., Corbineau, F., Theodoulou, F. L., Bailey-Serres, J., and Holdsworth, M. J. (2011) Homeostatic response to hypoxia is regulated by the N-end rule pathway in plants. *Nature* **479,** 415–418 CrossRef Medline
32. Licausi, F., Kosmacz, M., Weits, D. A., Giuntoli, B., Giorgi, F. M., Voesenek, L. A., Perata, P., and van Dongen, J. T. (2011) Oxygen sensing in plants is mediated by an N-end rule pathway for protein destabilization. *Nature* **479,** 419–422 CrossRef Medline

33. Giglione, C., Vallon, O., and Meinnel, T. (2003) Control of protein lifespan by N-terminal methionine excision. *EMBO J.* **22,** 13–23 CrossRef Medline
34. Chen, S., Vetro, J. A., and Chang, Y. H. (2002) The specificity *in vivo* of two distinct methionine aminopeptidases in *Saccharomyces cerevisiae*. *Arch Biochem. Biophys.* **398,** 87–93 CrossRef Medline
35. Tasaki, T., Mulder, L. C., Iwamatsu, A., Lee, M. J., Davydov, I. V., Varshavsky, A., Muesing, M., and Kwon, Y. T. (2005) A family of mammalian E3 ubiquitin ligases that contain the UBR box motif and recognize N-degrons. *Mol. Cell. Biol.* **25,** 7120–7136 CrossRef Medline
36. Lim, B., Jun, H. J., Kim, A. Y., Kim, S., Choi, J., and Kim, J. (2012) The TFG-TEC fusion gene created by the t(3;9) translocation in human extraskeletal myxoid chondrosarcomas encodes a more potent transcriptional activator than TEC. *Carcinogenesis* **33,** 1450–1458 CrossRef Medline
37. Turner, G. C., and Varshavsky, A. (2000) Detecting and measuring co-translational protein degradation *in vivo*. *Science* **289,** 2117–2120 CrossRef Medline
38. Qian, S. B., Princiotta, M. F., Bennink, J. R., and Yewdell, J. W. (2006) Characterization of rapidly degraded polypeptides in mammalian cells reveals a novel layer of nascent protein quality control. *J. Biol. Chem.* **281,** 392–400 CrossRef Medline
39. Schubert, U., Antón, L. C., Gibbs, J., Norbury, C. C., Yewdell, J. W., and Bennink, J. R. (2000) Rapid degradation of a large fraction of newly synthesized proteins by proteasomes. *Nature* **404,** 770–774 CrossRef Medline
40. Schild, D., Glassner, B. J., Mortimer, R. K., Carlson, M., and Laurent, B. C. (1992) Identification of RAD16, a yeast excision repair gene homologous to the recombinational repair gene RAD54 and to the SNF2 gene involved in transcriptional activation. *Yeast* **8,** 385–395 CrossRef Medline
41. Polevoda, B., Cardillo, T. S., Doyle, T. C., Bedi, G. S., and Sherman, F. (2003) Nat3p and Mdm20p are required for function of yeast NatB Nα-terminal acetyltransferase and of actin and tropomyosin. *J. Biol. Chem.* **278,** 30686–30697 CrossRef Medline
42. Bonissone, S., Gupta, N., Romine, M., Bradshaw, R. A., and Pevzner, P. A. (2013) N-terminal protein processing: a comparative proteogenomic analysis. *Mol. Cell. Proteomics* **12,** 14–28 CrossRef Medline
43. Walker, K. W., and Bradshaw, R. A. (1999) Yeast methionine aminopeptidase I. Alteration of substrate specificity by site-directed mutagenesis. *J. Biol. Chem.* **274,** 13403–13409 CrossRef Medline
44. Meinnel, T., and Giglione, C. (2008) Tools for analyzing and predicting N-terminal protein modifications. *Proteomics* **8,** 626–649 CrossRef Medline
45. Kats, I., Khmelinskii, A., Kschonsak, M., Huber, F., Kniess, R. A., Bartosik, A., and Knop, M. (2018) Mapping degradation signals and pathways in a eukaryotic N-terminome. *Mol. Cell* **70,** 488–501.e5 CrossRef Medline
46. Ghislain, M., Dohmen, R. J., Levy, F., and Varshavsky, A. (1996) Cdc48p interacts with Ufd3p, a WD repeat protein required for ubiquitin-mediated proteolysis in *Saccharomyces cerevisiae*. *EMBO J.* **15,** 4884–4899 CrossRef Medline
47. Sadis, S., Atienza, C., Jr., and Finley, D. (1995) Synthetic signals for ubiquitin-dependent proteolysis. *Mol. Cell. Biol.* **15,** 4086–4094 CrossRef Medline
48. Kim, J. M., and Hwang, C. S. (2014) Crosstalk between the Arg/N-end and Ac/N-end rule. *Cell Cycle* **13,** 1366–1367 CrossRef Medline
49. Zattas, D., Adle, D. J., Rubenstein, E. M., and Hochstrasser, M. (2013) N-terminal acetylation of the yeast Derlin Der1 is essential for Hrd1 ubiquitin-ligase activity toward luminal ER substrates. *Mol. Biol. Cell* **24,** 890–900 CrossRef Medline
50. Kim, I., Miller, C. R., Young, D. L., and Fields, S. (2013) High-throughput analysis of *in vivo* protein stability. *Mol. Cell. Proteomics* **12,** 3370–3378 CrossRef Medline
51. Neal, S., Jaeger, P. A., Duttke, S. H., Benner, C., Glass, C. K., Ideker, T., and Hampton, R. Y. (2018) The Dfm1 Derlin is required for ERAD retrotranslocation of integral membrane proteins. *Mol. Cell* **69,** 915 CrossRef Medline
52. Sato, B. K., and Hampton, R. Y. (2006) Yeast Derlin Dfm1 interacts with Cdc48 and functions in ER homeostasis. *Yeast* **23,** 1053–1064 CrossRef Medline
53. Goder, V., Carvalho, P., and Rapoport, T. A. (2008) The ER-associated degradation component Der1p and its homolog Dfm1p are contained in complexes with distinct cofactors of the ATPase Cdc48p. *FEBS Lett.* **582,** 1575–1580 CrossRef Medline
54. Avci, D., Fuchs, S., Schrul, B., Fukumori, A., Breker, M., Frumkin, I., Chen, C. Y., Biniossek, M. L., Kremmer, E., Schilling, O., Steiner, H., Schuldiner, M., and Lemberg, M. K. (2014) The yeast ER-intramembrane protease Ypf1 refines nutrient sensing by regulating transporter abundance. *Mol. Cell* **56,** 630–640 CrossRef Medline
55. Stolz, A., Schweizer, R. S., Schäfer, A., and Wolf, D. H. (2010) Dfm1 forms distinct complexes with Cdc48 and the ER ubiquitin ligases and is required for ERAD. *Traffic* **11,** 1363–1369 CrossRef Medline
56. Hanna M. G., 4th., Block, S., Frankel, E. B., Hou, F., Johnson, A., Yuan, L., Knight, G., Moresco, J. J., Yates, J. R., 3rd., Ashton, R., Schekman, R., Tong, Y., and Audhya, A. (2017) TFG facilitates outer coat disassembly on COPII transport carriers to promote tethering and fusion with ER-Golgi intermediate compartments. *Proc. Natl. Acad. Sci. U.S.A.* **114,** E7707–E7716 CrossRef Medline
57. Hernández, L., Pinyol, M., Hernández, S., Beà, S., Pulford, K., Rosenwald, A., Lamant, L., Falini, B., Ott, G., Mason, D. Y., Delsol, G., and Campo, E. (1999) TRK-fused gene (TFG) is a new partner of ALK in anaplastic large cell lymphoma producing two structurally different TFG-ALK translocations. *Blood* **94,** 3265–3268 Medline
58. Hisaoka, M., Ishida, T., Imamura, T., and Hashimoto, H. (2004) TFG is a novel fusion partner of NOR1 in extraskeletal myxoid chondrosarcoma. *Genes Chromosomes Cancer* **40,** 325–328 CrossRef Medline
59. Miranda, C., Roccato, E., Raho, G., Pagliardini, S., Pierotti, M. A., and Greco, A. (2006) The TFG protein, involved in oncogenic rearrangements, interacts with TANK and NEMO, two proteins involved in the NF-κB pathway. *J. Cell. Physiol.* **208,** 154–160 CrossRef Medline
60. Sherman, F. (2002) Getting started with yeast. *Methods Enzymol.* **350,** 3–41 CrossRef Medline
61. Gietz, R. D. (2014) Yeast transformation by the LiAc/SS carrier DNA/PEG method. *Methods Mol. Biol.* **1163,** 33–44 CrossRef Medline